Dalton Transactions

Photocatalytic Hydrogen Evolution Using a Ru(II)-Bound Heteroaromatic Ligand as a Reactive Site

Journal:	*Dalton Transactions*
Manuscript ID	DT-ART-10-2020-003546.R1
Article Type:	Paper
Date Submitted by the Author:	06-Nov-2020

Complete List of Authors:	Sawaki, Takuya; Department of Chemistry/University of Tsukuba Ishizuka, Tomoya; Department of Chemistry/University of Tsukuba Namura, Nanase; University of Tsukuba, Department of Chemistry Hong, Dachao; National Institute of Advanced Industrial Science and Technology (AIST) Miyanishi, Mayuko; Institute for Materials Chemistry and Engineering, Kyushu University and CREST (JST) Shiota, Yoshihito; Institute for Materials Chemistry and Engineering, Kyushu University and CREST (JST) Kotani, Hiroaki; Department of Chemistry/University of Tsukuba Yoshizawa, Kazunari; Institute for Materials Chemistry and Engineering, Kyushu University and CREST (JST) Jung, Jieun; Department of Chemistry and Nano Science/Ewha Womans University Fukuzumi, Shunichi; Department of Chemistry and Nano Science/Ewha Womans University Kojima, Takahiko; University of Tsukuba, Department of Chemistry

ARTICLE

Photocatalytic Hydrogen Evolution Using a Ru(II)-Bound Heteroaromatic Ligand as a Reactive Site

Received 00th January 20xx,
Accepted 00th January 20xx

DOI: 10.1039/x0xx00000x

Takuya Sawaki,[a] Tomoya Ishizuka,[a] Nanase Namura,[a] Dachao Hong,[a,b] Mayuko Miyanishi,[c] Yoshihito Shiota,[c] Hiroaki Kotani,[a] Kazunari Yoshizawa,*[c] Jieun Jung,[d] Shunichi Fukuzumi[d,e] and Takahiko Kojima*[a]

A Ru^{II} complex, $[Ru^{II}(tpphz)(bpy)_2]^{2+}$ (**1**) (tpphz = tetrapyridophenazine, bpy = 2,2′-bipyridine), whose tpphz ligand has a pyrazine moiety, is converted efficiently to $[Ru^{II}(tpphz\text{-}HH)(bpy)_2]^{2+}$ (**2**) having a dihydropyrazine moiety upon photoirradiation of a water-methanol mixed solvent solution of **1** in the presence of an electron donor in 30% quantum yield. In this reaction, the triplet metal-to-ligand charge-transfer excited state (^{3}MLCT*) of **1** is firstly formed upon photoirradiation and the ^{3}MLCT* state is reductively quenched with an electron donor to afford $[Ru^{II}(tpphz^{\bullet-})(bpy)_2]^{+}$, which is converted to **2** without observation of detectable reduced intermediates by nano-second laser flash photolysis. An inverse kinetic isotope effect (KIE) was observed to be 0.63 in the N-H bond formation of **2** at the dihydropyrazine moiety. White-light (380 – 670 nm) irradiation to a solution of **1** in a protic solvent, in the presence of an electron donor under inert atmosphere, afforded photocatalytic H_2 evolution and hydrogenation of organic substrates. In the reactions, complex **2** is required to be excited to form its ^{3}MLCT* state to react with a proton and aldehydes. In the photocatalytic H_2 evolution, the H-H bond formation between the photoexcited **2** and a proton is involved in the rate-determining step with showing normal KIE to be 5.2 on H_2 evolving rates. Density functional theory (DFT) and time-dependent DFT (TD-DFT) calculations on the reaction mechanism of H_2 evolution from the ground and photo-excited states of **2** were perfomed to have a better understanding of the photocatalytic processes.

Introduction

Photocatalytic reduction promoted by visible light to produce chemical energy sources such as H_2[1-3] and to perform chemical conversion of organic substrates to useful products[4] has been considered as one of important processes toward construction of a sustainable society.[5] As a method to perform the reactions under mild conditions with visible-light irradiation, a robust and efficient photosensitizer, which exhibits a strong absorption band in the visible region, has been required to the photoexcited state of a photosensitizer that acts as an electron acceptor.[6]

Among organic and inorganic photosensitizers, ruthenium(II) complexes having diimine chelating ligands have been proven to be effective and useful in many kinds of photoinduced reactions.[7] Relatively long-lived triplet metal-to-ligand charge transfer (^{3}MLCT*) excited states of Ru^{II}-diimine complexes have been extensively utilised for various photoinduced catalytic reactions.[8-10] Among the Ru^{II}-diimine complexes, $[Ru^{II}(bpy)_3]^{2+}$ (bpy = 2,2′-bipyridine) has been most frequently employed as a photosensitizing reagent for various photocatalytic reactions by virtue of the long-lived ^{3}MLCT* state.[11-21] The ^{3}MLCT* state of $[Ru^{II}(bpy)_3]^{2+}$ has been known to exhibit dichotomic reactivity, *i.e.*, oxidative quenching to release an electron to an electron acceptor to form $[Ru^{III}(bpy)_3]^{3+}$ and also reductive quenching to accept an electron from an electron donor to afford $[Ru^{II}(bpy^{\bullet-})(bpy)_2]^{+}$ (Scheme 1).[11] A versatile oxidative quenching method involves

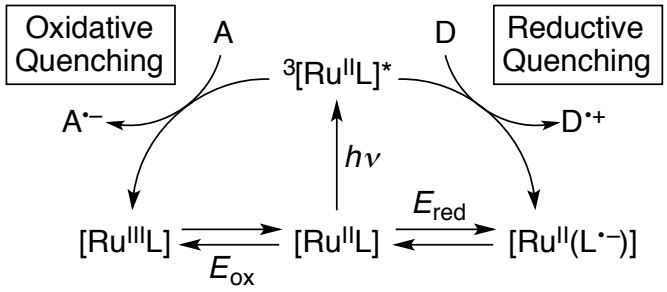

Scheme 1 Schematic description of photoinduced ET reactions of a Ru^{II}-diimine complex. L: diimine ligand, D: electron donor, A: electron acceptor, E_{ox}: the first oxidation potential, E_{red}: the first reduction potential.

[a] *Department of Chemistry, Faculty of Pure and Applied Sciences, University of Tsukuba and CREST (JST), 1-1-1 Tennoudai, Tsukuba, Ibaraki 305-8571, Japan.*
[b] *Interdisciplinary Research Centre for Catalytic Chemistry, National Institute of Advanced Industrial Science and Technology (AIST), 1-1-1 Higashi, Tsukuba, Ibaraki 305-8565, Japan.*
[c] *Institute for Materials Chemistry and Engineering, Kyushu University, Motooka, Nishi-Ku, Fukuoka 819-0395, Japan.*
[d] *Department of Chemistry and Nano Science, Ewha Womans University, Seoul 120-750, South Korea.*
[e] *Faculty of Science and Technology, Meijo University, Nagoya, Aichi 468-8502, Japan.*
Electronic Supplementary Information (ESI) available: See DOI: 10.1039/x0xx00000x

an electron acceptor such as $[Co^{III}Cl(NH_3)_5]^{2+}$ to form $[Ru^{III}(bpy)_3]^{3+}$ (E_{red} = +1.26 V *vs.* NHE), which can act as a powerful oxidant to generate reactive species such as high-valent metal-oxo complexes in photocatalytic oxidation reactions[16,17] and also water oxidation.[18] On the other hand, the ^{3}MLCT* state of $[Ru^{II}(bpy)_3]^{2+}$ can be reductively quenched in the presence of an electron donor such as triethylamine to afford $[Ru^{II}(bpy^{\bullet-})(bpy)_2]^+$ (E_{ox} = –1.28 V *vs.* NHE), which can serve as a strong reductant to afford reactive species in photocatalytic reduction reactions, including hydrogen evolution[19,20] and reductive conversion of organic compounds.[21]

In the case of the reductive quenching of the ^{3}MLCT* state of Ru^{II}-diimine complexes, ET reactions afford Ru^{II} complexes having an unpaired electron in the ligand π-systems as 1e$^-$-reductants. Since, in most cases, radical intermediates that are formed through 1e$^-$-reduction of substrates by the 1e$^-$-reduced Ru^{II}-diimine complexes lower the product selectivity, it is very useful to lead the ^{3}MLCT* state of Ru^{II} complexes to stable forms having no unpaired electrons.[22] As one of plausible strategies, we focused on proton-coupled electron transfer (PCET) from an electron donor to the ^{3}MLCT* state of a Ru^{II}-diimine complex having two proton-accepting sites. In the presence of proton and electron donors in a close contact to a protonated 1e$^-$-reduced complex ($Ru^{II}(HL^{\bullet})$), the complex can undergo further reduction and protonation to generate a 2H (2H$^+$/2e$^-$)-reduced species ($Ru^{II}(H_2L)$).[22-26] PCET allows us to stabilize the 2e$^-$ reduction products and also to lower the potential barriers of the reduction reactions in comparison with ET without proton transfer (PT) or PT without ET.[24] Tanaka and co-workers have demonstrated photoinduced PCET reactions to obtain Ru^{II} complexes having 2H-reduced ligands with use of two-proton and 2e$^-$ accepting ligands such as 2-(2-pyridyl)benzo[b]-1,5-naphthyridine to generate an analogue of reduced nicotinamide adenine dinucleotide (NADH) involving both C-H and N-H bond formation.[22,27] They have also demonstrated that the 2H-reduced Ru^{II} complex can perform hydride transfer to external substrates such as carbon dioxide[27d] and dioxygen.[22c]

In this study, we have used a Ru^{II} complex with a π-expanded heteroaromatic diimine ligand having a pyrazine moiety, tetrapyrido[3,2-*a*:2′,3′-*c*:3″,2″-*h*:2‴,3‴-*j*]phenazine (tpphz) for photocatalytic hydrogen evolution. The pyrazine moiety of the tpphz ligand is expected to function as a 2H$^+$ and 2e$^-$ acceptor, since the pyrazine moiety can be 2H-reduced to afford a dihydropyrazine derivative by accepting two protons at the two nitrogen atoms and two-electrons in a π* orbital; dihydropyrazine and its derivatives possess high reduction ability to turn back to the corresponding pyrazine derivatives by transferring two protons and two electrons to substrates by virtue of the aromatization as a driving force.[28,29] Herein, we describe photochemical reduction of the Ru^{II}-tpphz complex (**1**; Chart 1) with use of an electron donor such as triethylamine (Et_3N) to afford a Ru^{II} complex with a reduced tpphz ligand, whose pyrazine moiety is dihydrogenated.

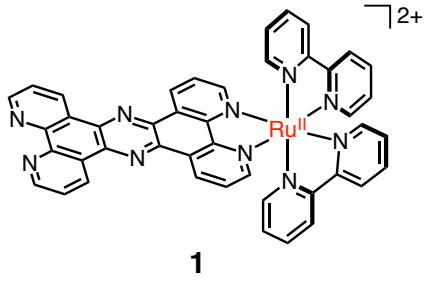

1

Chart 1 Molecular structure of the photocatalyst **1**.

Mechanistic insights into photocatalytic hydrogen evolution by complex **1** in the presence of an electron donor is also presented. Thus, the catalytically active site of **1** is not the Ru centre but the π-expanded heteroaromatic diimine ligand in the hydrogen evolution.[30] Furthermore, complex **1** also shows photocatalytic activity toward hydrogenation of organic substrates such as benzaldehyde.

Results and discussion

Electrochemical measurements and phosphorescence quenching of 1.

The Ru^{II} complex, **1**,[31,32] having two bpy molecules and one tpphz molecule as ligands, has been mainly employed in this study (Chart 1). As a counter anion of the complex, perchlorate was chosen to ensure the reasonable solubility into aqueous media. In the cyclic and differential-pulse voltammograms (CV and DPV, respectively) of **1**·$(ClO_4)_2$ in acetonitrile (CH_3CN) containing 0.1 M tetrabutylammonium hexafluorophosphate ($TBAPF_6$) as an electrolyte, reduction waves were observed at –0.98 and –1.12 V *vs.* SCE (Fig. S1), the former of which was assigned to the reduction of the tpphz ligand and the latter was to that of a bpy ligand.[32,33]

To explore the photochemical properties of **1**, the reductive quenching of the triplet MLCT excited state of **1** (^{3}**1***)[34] was investigated with use of various electron donors. The emission spectrum of **1**·$(ClO_4)_2$ with the excitation wavelength at 424 nm in the absence of reductants in a water-CH_3OH mixed solvent (1 : 1, v/v) exhibited phosphorescence centred at 634 nm at room temperature (Fig. S2; black line). Upon addition of Et_3N (1.8 M) as an electron donor, the phosphorescence was quenched by 76% (Fig. S2; red line); hence, ^{3}**1*** can be efficiently quenched by Et_3N. The quenching efficiency with Et_3N was investigated on the basis of the Stern-Volmer analysis[35] (Fig. S3). The relative phosphorescence intensity (I_0/I) was plotted against the Et_3N concentration, which resulted in a linear relationship (Fig. S3a), and the Stern-Volmer equation ($I_0/I = k_q\tau_0[Et_3N] + 1$) was applied to obtain the quenching rate constant, k_q. The quenching constant ($k_q\tau_0$) was determined to be 0.23 M^{-1} from the slope of the plot and the lifetime of the triplet excited state of **1** was determined to be 16.7 ns from the decay curve of the emission intensity (Fig. S3b). Therefore, the k_q value was determined to be 1.4×10^7 M^{-1} s^{-1}.

For seeking a better electron donor, phosphorescence quenching efficiencies were determined with use of other

reductants (Table S1). Among the electron donors examined in this work, L-ascorbic acid (As) and oxalic acid (Ox) exhibited comparable quenching efficiencies to that with Et_3N; 89% for As and 61% for Ox, and *N*-ethylmorpholine (EtMor) performed quenching with lower efficiency of 12%. Ferrocene (Fc) as a reductant also showed weakened phosphorescence of **1**. However, interference in light absorption of **1** by the absorption of Fc was very severe in the visible region (ε = 82 for Fc at λ_{max} = 440 nm), because a large excess amount of Fc, 1000 equiv relative to **1**·$(ClO_4)_2$, was used in the experiment; thus, the incident light should be exclusively absorbed by Fc. Therefore, the quenching efficiencies could not be estimated correctly. The quenching efficiencies of Et_3N, As, Ox, and EtMor can be elucidated by relation between the oxidation potentials (E_{ox}) of the reductants and the reduction potential (E_{red}) of ^{3}**1***; the calculated E_{red} of ^{3}**1*** is +1.06 V *vs.* SCE, and thus, ^{3}**1*** can be quenched by Et_3N (E_{ox} = +0.80 V *vs.* SCE), As (+0.15), Ox (+0.98) and EtMor (> +1.0), judging from the E_{ox} values obtained from DPV measurements (Fig. S4). Additionally, as E_{ox} of the reductant lowers, the quenching efficiency becomes higher, due to the increase in the driving force of ET from the reductants to ^{3}**1***.

Characterization of the photochemical product obtained from 1.

To monitor the photochemical reaction of **1** in the presence of Et_3N as an electron donor, UV-Vis and ^{1}H NMR spectroscopies were applied. Complex **1**·$(ClO_4)_2$ exhibited an MLCT absorption band at 450 nm and a π-π* transition band of the tpphz ligand around 380 nm in a water-CH_3OH mixed solvent (1 : 1, v/v) containing Et_3N (1.8 M) (light-blue trace in Fig. 1). Under photoirradiation with the white light (380 – 670 nm) to the solution of **1**·$(ClO_4)_2$, the π-π* transition band, observed around 380 nm, gradually decreased and the MLCT band gradually increased, concomitant with the appearance of a broad absorption band in the range of 500 – 800 nm (red trace in Fig. 1); the broad lower-energy absorption band could be assigned to that due to decomposed products derived from 1e$^-$-oxidized Et_3N.[36] The disappearance of the π-π* transition band of the tpphz moiety indicates shrinkage of the π-conjugation circuit expanding to the whole tpphz ligand. The change was completed within 10 min, and the quantum yield of the change with incident light at 440 nm was determined to be 30% by a typical actinometer method.[37] This quantum yield is quite high for this kind of photochemical reactions.[27a,38] Similar spectral changes including decrease in π-π* transition around 380 nm were observed with use of other reductants (Fig. S5).[39,40] In addition, a similar spectral change was also observed in the case of the electrolytic reduction at –1.4 V *vs.* Ag/AgCl in the presence of tetramethylammonium chloride (Me_4NCl) as an electrolyte in a CH_3OH-borate buffer (pH 9.5) mixed solvent (1 : 1, v/v) (Fig. S8).

Photoirradiation of a D_2O-CD_3OD mixed solvent solution (1 : 1, v/v) of **1**·$(ClO_4)_2$ (0.3 mM) and Et_3N (71 mM) with white light (380 – 670 nm) resulted in upfield shifts of the ^{1}H NMR signals of the tpphz ligand in **1**, whereas those of the bpy ligands were almost intact (Fig. 2). This photoreaction proceeded quantitatively, since no signals due to side products were observed in the spectrum. Small shifts of the ^{1}H NMR signals ascribable to those of the bpy ligands after photo-irradiation also support that the valence number (2+) of the Ru centre and the total charge of the cationic moiety of the complex are intact after the photoreduction of the tpphz ligand.

The N*H* atoms of the reduced pyrazine moiety in the reduced form (**2**) cannot be observed by ^{1}H NMR spectroscopy in deuterated protic solvents due to the fast H/D exchange with deuterated protic solvents. Therefore, to confirm the hybridization change of the two nitrogen atoms of the pyrazine moiety from **1** to **2**, ^{15}N NMR spectra were measured using (**1**-^{15}N)·Cl_2, whose two nitrogen atoms in the pyrazine

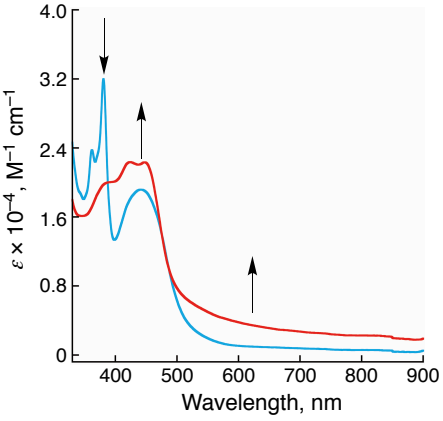

Fig. 1 UV-Vis spectral change under photoirradiation (380 – 670 nm) to the solution of **1**·$(ClO_4)_2$ (25 μM) in a water-CH_3OH-Et_3N mixed solvent (1 : 1 : 1, v/v/v) at room temperature: before photoirradiation (light-blue trace) and after 10 min irradiation (red trace). Before the photoirradiation, the solution pH was measured with a digital pH meter to be 12.1.

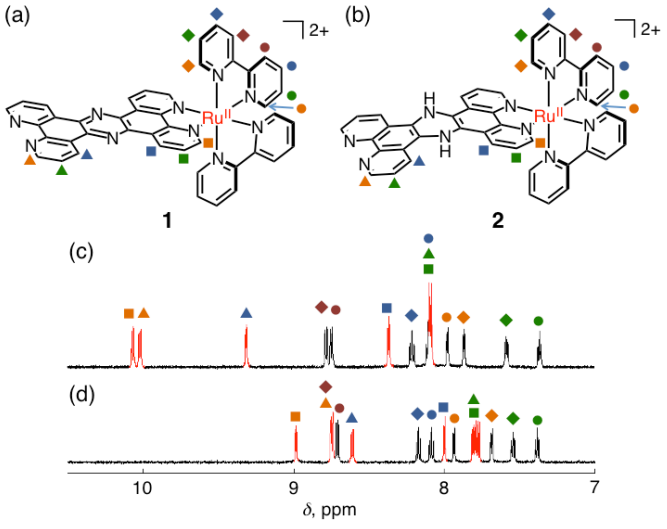

Fig. 2 Molecular structures of **1** (a) and **2** (b). ^{1}H NMR spectra of **1**·$(ClO_4)_2$ (0.3 mM) in a D_2O-CD_3OD mixed solvent (1:1, v/v) in the presence of Et_3N (71 mM) (c) and after photoirradiation with white light (380 – 670 nm) for 30 min at room temperature (d). The red signals indicate those derived from the hydrogen atoms of the tpphz moiety, and the symbols indicate the positions of protons in the structures of **1** and **2** shown above.

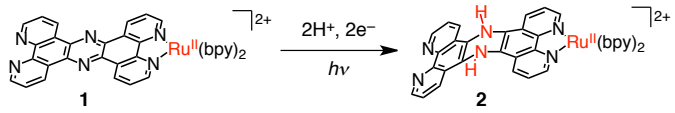

Scheme 2 Photoinduced PCET reduction of **1**.

moiety of the tpphz ligand were labelled with ^{15}N (98%), under high concentration conditions. Note that, to improve the solubility of **1**-^{15}N in CH_3OH, Cl^- ions were employed as the counter ions in place of ClO_4^-. In the ^{15}N NMR spectrum of (**1**-^{15}N)·Cl_2, a singlet signal was observed at δ 308.22 ppm, calibrated with an external reference of $(NH_4)_2SO_4$ (20.55 ppm),[41] at room temperature (Fig. 3a). On the other hand, after the white-light irradiation of a CH_3OH solution of (**1**-^{15}N)·Cl_2 for 4 h in the presence of Et_3N (71 mM), the ^{15}N NMR signal was shifted to 68.86 ppm at room temperature (Fig. 3b and c). These results indicate that the hybridization of the N atoms of the pyrazine moiety is changed from sp^2 to sp^3 hybridization in the course of the photochemical reduction. Thus, we propose that the reduced product **2** is a Ru(II) complex having a dihydropyrazine moiety as shown in Scheme 2. Upon lowering the temperature to 195 K, the ^{15}N NMR signal of (**2**-^{15}N)·Cl_2 was shifted to 73.43 ppm and the signal was split into a doublet due to coupling with a ^1H nucleus (J_{NH} = 81.6 Hz), indicating that the ^{15}N atoms at the pyrazine moiety in the photochemical product (**2**-^{15}N)·Cl_2 connect directly to one H atom (Fig. 3d). These observations strongly support the hydrogenation of the pyrazine nitrogen atoms of the tpphz ligand as the results of photoinduced PCET, in which protons are derived from the solvent (MeOH) and electrons are from Et_3N.

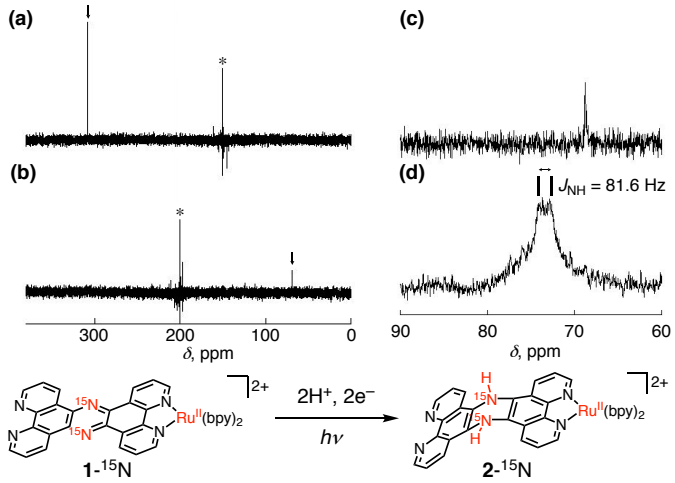

Fig. 3 ^{15}N NMR spectra in a CH_3OH-benzene-d_6 mixed solvent (9 : 1, v/v) of (**1**-^{15}N)·Cl_2 (a) and after photoirradiation (380 – 670 nm) in the presence of Et_3N at room temperature (b and c) and at 195 K (d). Arrows in (a) and (b) indicates the signals assigned to the ^{15}N atoms of the pyrazine moiety of **1**-^{15}N and the corresponding ^{15}N atom of the photochemical product, **2**-^{15}N, respectively. *: artefact at the frequency centre.

In addition, complex **2**·$(ClO_4)_2$ is highly air-sensitive: Once it was exposed to air, it immediately turned back to **1**,

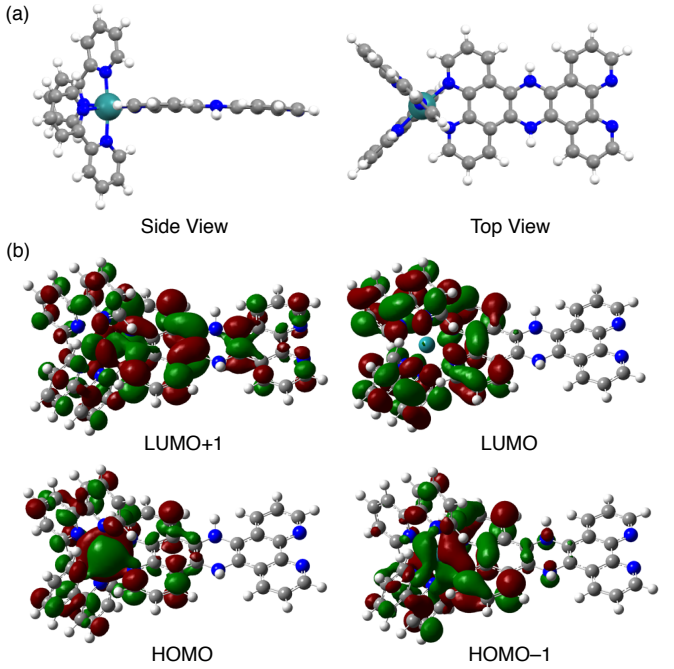

Fig. 4 DFT calculations on **2** at the B3LYP level of theory in vacuum: (a) optimized structure of **2** and (b) frontier MOs of **2**.

exemplifying the high reactivity of **2** as a reductant (Fig. S9). After quenching **2**·$(ClO_4)_2$ with air, the solution was analysed with iodometry. When an NaI solution was added to the reaction mixture after the exposure to dioxygen, the absorbance around 350 nm did not increase (Fig. S10). If the solution contains H_2O_2, absorption around 350 nm should appear due to I_3^- formed by oxidation of I^- with H_2O_2.[42] The lack of the absorption around 350 nm due to I_3^- after the treatment of the solution with NaI indicates that the product from the reaction of O_2 with **2** is not H_2O_2. In addition, another attempt to detect H_2O_2 was also made with $[Ti^{IV}(O)(TPyPH_4)]^{4+}$ (TPyP = 5,10,15,20-tetra(4-pyridyl)porphyrinato) (Fig. S11);[43] however, no significant absorption change was observed on the basis of a reaction with H_2O_2 and $[Ti^{IV}(O)(TPyPH_4)]^{4+}$ to rule out the formation of H_2O_2.

Density functional theory (DFT) calculations were performed to optimize the geometry of **2** at the B3LYP level of theory[44-46] combined with the SDD basis set[47] for the Ru atom and the D95** basis set[48] for the other atoms. The reduced tpphz ligand is very slightly distorted and the N*H* atoms are slightly deviated from the tpphz plane to the same direction (Fig. 4). Additionally, the LUMO is localized to the two bpy ligands and the Ru-side phenanthlorine moiety of the reduced tpphz ligand, and the π-conjugation on the whole tpphz moiety, as observed in **1**,[32b] disappears after the reduction (Fig. 4b). This is consistent with the fact that the π-π* transition band around 380 nm, derived from the tpphz ligand, weakened in the course of the photochemical reduction (Fig. 1).

Kinetic studies on the photochemical formation of 2.

To gain mechanistic insights into the formation of **2**,

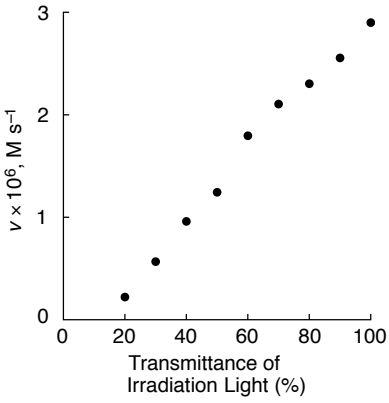

Fig. 5 A plot of the initial rates of the formation of **2**·$(ClO_4)_2$ from **1**·$(ClO_4)_2$ through a photochemical process against transmittance of irradiation light. The reactions were performed in a CH_3OH-H_2O mixed solvent solution (3 mL, 1 : 1, v/v) of **1**·$(ClO_4)_2$ (25 μM) in the presence of Et_3N (1 mL) under irradiation of white light (380 – 670 nm). The transmittance of irradiation light was controlled by a ND-filter equipped to the light source unit. The initial rates were obtained from the linear analysis on the basis of the absorbance changes at 380 nm.

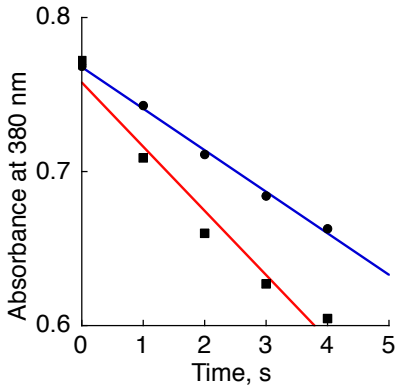

Fig. 6 Absorbance change at 380 nm in the initial step of the photo-chemical reduction of **1**·$(ClO_4)_2$ (25 μM) with Et_3N (1.8 M) in H_2O-CH_3OH (1 : 1, v/v, filled circles, blue line) and D_2O-CD_3OD (1 : 1, v/v, filled squares, red line) mixed solvents under photoirradiation (λ = 420 nm) at 297 K.

dependence of the rate (v) of the photochemical process on the concentration of **1** and on the irradiation power were explored. The progress of the reaction was monitored with the change of absorbance at 380 nm, which derives from the π-π* transition in the tpphz ligand of **1**. The rate of the formation of **2**·$(ClO_4)_2$ was determined to be 2.4×10^{-7} M s^{-1}, when the initial concentration of **1** was 10 μM. The v value increased in accordance with an increase in the concentration of **1**·$(ClO_4)_2$ in the range of 0 – 60 μM, showing saturation behaviour around 60 μM (Fig. S12). Also, the irradiation power of a light source affected the formation rate of **2**·$(ClO_4)_2$; a linear dependence of the v value was observed on the irradiation power of white light controlled by ND-filter (Fig. 5). The linear irradiation-power dependence indicates that the photochemical process to form **2** proceeds as a unimolecular reaction of **1** working as a photocatalyst, rather than a bimolecular reaction such as disproportionation between two molecules of 1e$^-$-reduced **1**. In addition, the saturation behaviour observed in Fig. S12 can be explained by the fact that the concentration of photoexcited **1** (**1***) is dominant for determining the rate in photochemical formation of **2**.

To investigate kinetic isotope effect (KIE) on the formation of **2**·$(ClO_4)_2$, photoirradiation of H_2O-CH_3OH and D_2O-CD_3OD mixed solvent solutions of **1**·$(ClO_4)_2$ in the presence of Et_3N as an electron donor was performed using the white light. The progress of the reaction was monitored by the change in absorbance at 380 nm, which derives from the π-π* transition in the tpphz ligand of **1** (Fig. 6). The reaction in the deuterated solvent proceeded faster than that in the non-deuterated solvent; the initial rate in the non-deuterated solvent (v_H) was determined to be 0.88×10^{-6} M s^{-1} and that in the deuterated solvent (v_D) was 1.4×10^{-6} M s^{-1}. Thus, the KIE value (v_H/v_D) was determined to be 0.63 for the formation of **2**·$(ClO_4)_2$. Additionally, the quantum yield in the deuterated solvent (Φ_D) was higher than that in the non-deuterated solvent (Φ_H): Φ_H = 0.30 and Φ_D = 0.48. The inverse KIE indicates that a bond-forming process involving an H atom (= $H^+ + e^-$) should occur in the rate-determining step (RDS) in the formation of **2**.[49] Therefore, the RDS in the photochemical formation of **2** should be the N-H bond formation at the pyrazine moiety. A similar inverse KIE (0.4) was reported for PCET from both toluene and $[Ru^{II}(bpy)_3]^{2+}$ to $[(N4Py)Fe^{IV}(O)]^{2+}$ (N4Py = *N*,*N*-bis(2-pyridylmethyl)-*N*-bis(2-pyridyl)methyl-amine), when HOTf was replaced by DOTf.[50]

Photocatalytic hydrogen evolution with 1·$(ClO_4)_2$ as a catalyst.

Further irradiation of a water-CH_3OH mixed solvent solution (1:1, v/v, 3 mL) of **1**·$(ClO_4)_2$ (25 μM) in the presence of Et_3N (1.8 M) as a sacrificial reductant with the white light (380 – 670 nm) for 6 h after forming **2** at room temperature resulted in evolution of 0.08 μmol of H_2 that was detected by gas chromatography (GC). No Ru nanoparticle formation was observed by dynamic light scattering (DLS) measurements (Fig. S13). The turnover number (TON) based on the catalyst **1** was determined to be 1. Therefore, complex **2**, formed in the first photochemical process, probably acts as an intermediate in the hydrogen evolution catalysed by **1**.[30,51] Photocatalytic hydrogen evolution was also performed with the other reductants employed for the reductive quenching experiments (see above); however, the amount of H_2 evolved was not related to the quenching efficiencies. Using Et_3N as the reductant afforded the highest rate of hydrogen evolution among them (Table S1). The low efficiency for As as a reductant is probably due to the back ET, because the redox process of As is exceptionally reversible among the reductants used in this study.[52] Dilution of the catalyst to 2.5 μM and further elongation of the reaction time to 380 h, 1.6 μmol of H_2 evolved was detected and then the TON was improved to 160. The highest TON was obtained with use of tri-ethanolamine as a reductant, and the TON of the hydrogen evolution was determined to be 620 for 380 h.

A photoelectrocatalytic reaction[53] was also performed to gain higher efficiency in hydrogen evolution. Firstly, dependence of the electric current on the irradiation of white light (380 – 670 nm) was examined in a CH_3OH-borate buffer (pH 9.5) mixed solvent solution (1 : 1, v/v) with a continuous

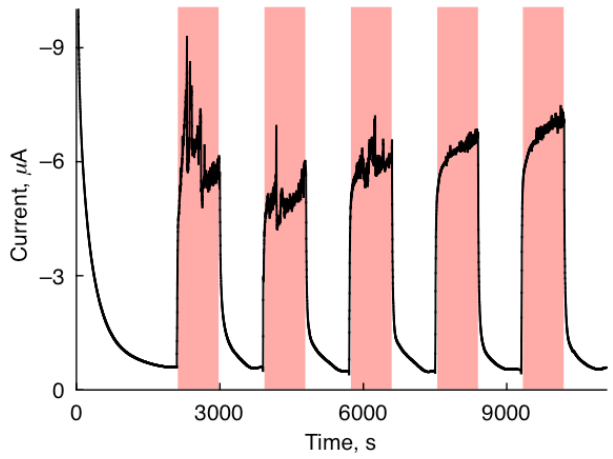

Fig. 7 Electric currents with (red background) and without (white background) photoirradiation of white light (380 – 670 nm) to the solution of **1**·$(ClO_4)_2$ (300 μM) in a CH_3OH-borate buffer (pH 9.5) mixed solvent (1:1, v/v), applying a continuous voltage at –1.4 V *vs.* Ag/AgCl on the working electrode. Working electrode: glassy carbon. Counter electrode: Pt wire. Reference electrode: Ag/AgCl.

voltage at –1.4 V *vs.* Ag/AgCl loaded on the GC disk electrode of 1.6 mm diameter as the working electrode (Fig. 7). The current clearly increased upon photoirradiation, indicating that a catalytic reaction can proceed in the presence of **1**·$(ClO_4)_2$ under photoirradiation accompanying bulk electrolysis. When photoirradiation with white light (380 – 670 nm) was performed for 3 h on the glassy-carbon working electrode surface (See the Experimental section), on which a continuous voltage was loaded at –1.40 V *vs.* Ag/AgCl in a CH_3OH-borate buffer (pH 9.5) mixed solvent solution (1 : 1, v/v, 5 mL) of **1**·$(ClO_4)_2$ (300 μM) containing no chemical electron donors, 76 μmol of hydrogen was evolved (total loaded charge: 13.1 C) and the TON based on the catalyst was determined to be 51. In contrast, only the electrolysis at the same applied voltage in the dark did not exhibit any hydrogen evolution. Additionally, only the photoirradiation without electrolysis did not afford any signs of hydrogen evolution. Therefore, both light irradiation and electrolysis are necessary for the hydrogen evolution by **1**·$(ClO_4)_2$.

Exploration of the catalytically active site in 1 for the hydrogen evolution.

To confirm the assumption that complex **2** is the active intermediate of the hydrogen evolution catalysed by **1**, the catalytic activity was examined for other four Ru^{II} complexes having similar structures to that of **1**. Complex **3**[54] with a π-expanded diimine ligand, in which the two nitrogen atoms at the *h*- and *j*-pyridine rings of the tpphz ligand are replaced by C-Hs (Fig. 8). $[Ru^{II}(bpy)_3]^{2+}$ (**4**; Fig. 8), and $[Ru^{II}(bpy)_2(bpm)]^{2+}$ (bpm = 2,2′-bipyrimidine, **5**; Fig. 8), the former of which had no diimine and pyrazine moieties but only a Ru^{II} centre and the latter of which had no pyrazine moiety but uncoordinated diimine one, were also examined as catalysts for hydrogen evolution under the same conditions as those applied to **1**. In consequence, complex **3**·$(ClO_4)_2$ exhibited the catalytic activity for hydrogen evolution with a comparable or slightly better efficiency as compared with that of **1**·$(ClO_4)_2$, whereas no hydrogen evolution was observed for complexes **4**·$(ClO_4)_2$ and **5**·$(ClO_4)_2$ (Fig. 9). Therefore, it is concluded that the active site of **1** for the catalytic hydrogen evolution is neither the Ru^{II} centre nor the terminal vacant diimine moiety, but the pyrazine moiety at the

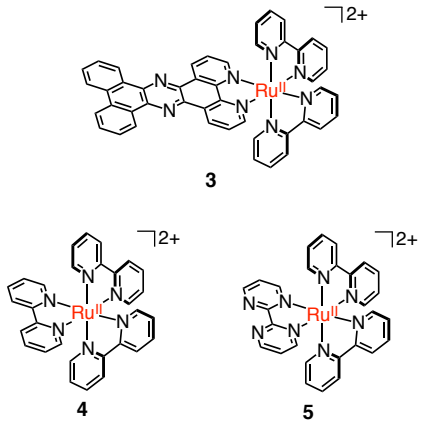

Fig. 8 Molecular structures of ruthenium(II)-polypyridine complexes, **3**, **4** and **5**.

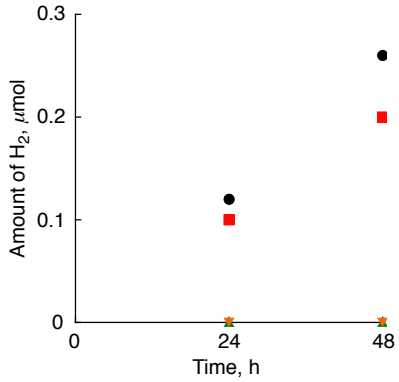

Fig. 9 Amount of dihydrogen evolved in the photocatalytic reaction (λ_{irr} = 380 – 670 nm) of **1**·$(ClO_4)_2$ (red filled square), **3**·$(ClO_4)_2$ (black filled circle), **4**·$(ClO_4)_2$ (orange triangle) and **5**·$(ClO_4)_2$ (green inverted-triangle). The concentration of the catalyst in the solution was set as 25 μM in a water-MeOH-Et_3N mixed solvent (1 : 1 : 1, v/v/v).

centre of the tpphz ligand in **1**. In addition, complex **3** also afforded a reduced intermediate (**6**), similar to **2**, under photoirradiation in the presence of Et_3N as an electron donor, as evidenced by the ^1H NMR spectral change (Fig. S14).

Mechanistic insights into photocatalytic hydrogen evolution by 1.

To confirm the reaction mechanism of the hydrogen evolution from the intermediate **2**, the dark reaction of **2** was explored. When the solution of **2**·$(ClO_4)_2$ was kept in the dark, the UV-Vis and ^1H NMR spectra indicated the recovery of **1**·$(ClO_4)_2$ from **2**·$(ClO_4)_2$. In the UV-vis spectral changes, the absorption from 400 to 900 nm initially increased (Fig. S15a), which was assigned to that due to decomposed products derived from $1e^-$-oxidized Et_3N.[36] Subsequently, the absorption assigned to the π-π* transition of the tpphz ligand recovered (Fig. S15b). Also in the ^1H NMR spectral changes, the signals due to **2**·$(ClO_4)_2$ were initially broadened, and subsequently, the

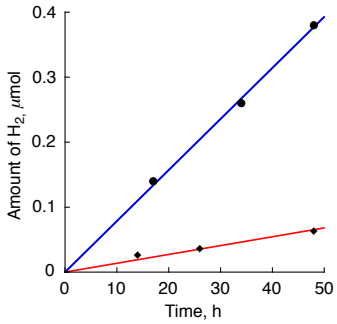

Fig. 10 The amount of H_2 evolved in the photocatalytic reaction with **1**·$(ClO_4)_2$ (25 μM) in H_2O-CH_3OH (filled circles, blue line) and D_2O-CD_3OD (filled diamonds, red line) mixed solvents (1 : 1, v/v), under photoirradiation of a white light (380 – 670 nm) at 297 K.

signals due to **1**·$(ClO_4)_2$ recovered (Fig. S16). The spectrum was completely changed into the same as the spectrum of **1**·$(ClO_4)_2$ after 86 h. During the dark reaction, however, hydrogen evolution was not observed at all, and the reaction rate of the dark reaction was very slow in comparison with those of the photocatalytic hydrogen evolution. Therefore, in the dark reaction, the recovery from **2** to **1** probably occurs through the reaction of **2** with decomposed products derived from 1e⁻-oxidized Et_3N formed in photoinduced ET from Et_3N to ^{3}**1***.[55] Thus, the hydrogen evolution process from the intermediate **2** requires further photoirradiation. This result matches to the fact that hydrogen evolution required both photoirradiation and electrolysis in the photoelectrocatalytic reaction, while the reaction did not occur only by the electrochemical reduction at the same potential (see above).

The amounts of H_2 evolved from the catalytic reactions were monitored using GC in both H_2O-CH_3OH and D_2O-CD_3OD mixed solvents (Fig. 10) under photoirradiation. In sharp contrast to the result of the photochemical process to form the intermediate **2**·$(ClO_4)_2$ (see above), the hydrogen evolution in the non-deuterated solvent was faster than that in the deuterated solvent. The initial rates were determined to be 7.8 nmol h^{-1} in the non-deuterated solvent and 1.5 nmol h^{-1} in the deuterated solvent, respectively, indicating the KIE value to be 5.2 for the final hydrogen evolution process from **2**·$(ClO_4)_2$. The rate of the H_2 evolution were much slower than those of the formation of **2**·$(ClO_4)_2$. Therefore, the RDS of the whole catalytic hydrogen evolution by **1**·$(ClO_4)_2$ is not the photochemical process to afford the intermediate **2**·$(ClO_4)_2$ but the hydrogen evolution process from **2**·$(ClO_4)_2$. The normal KIE observed in the hydrogen evolution process clearly indicates that the RDS in the process should be the cleavage of a bond involving a hydrogen atom.

Dependence of the hydrogen evolution rates on proton concentration was also investigated. With increasing the amount of $HClO_4$ added to the sample solution, the hydrogen evolution rates increased proportionally (Fig. S17). Thus, protons are involved in the hydrogen evolution process. Based on the observations, we propose that the hydrogen evolution occurs through an intermolecular coupling between a proton and one of NH of **2** as a hydride donor, followed by aromatization to recover the pyrazine moiety and simultaneous

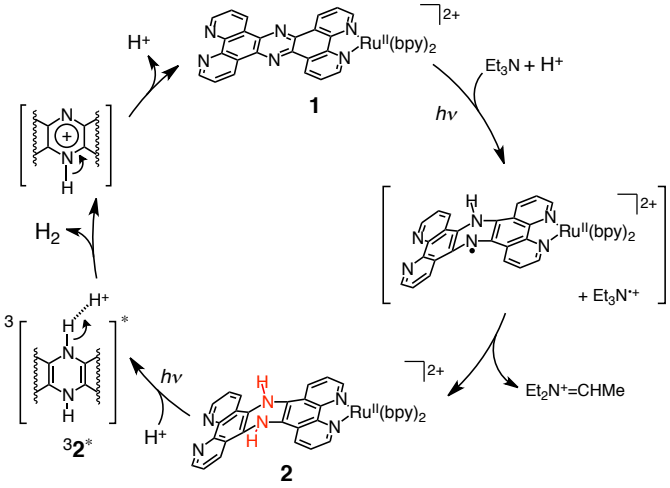

Scheme 3 A proposed reaction mechanism of the photocatalytic hydrogen evolution with **1**.

deprotonation of the remaining N-H proton to recover **1** (See Scheme 3).

Based on the results described above, we propose a plausible reaction mechanism of the photocatalytic hydrogen evolution with **1** in the presence of an electron donor in a CH_3OH-H_2O mixed solvent as shown in Scheme 3. The photoexcitation of **1** produces the ^{3}**1*** state as the first step, which is reductively quenched with Et_3N to afford a radical intermediate, $[Ru^{II}(tpphz^{•-})(bpy)_2]^+$. The reduced tpphz ligand in $[Ru^{II}(tpphz^{•-})(bpy)_2]^+$ catches a proton and an electron from 1e⁻-oxidized Et_3N ($Et_3N^{•+}$) in the solvent cage to generate the intermediate **2**.[22,27,38]

We performed CVs and DPVs of **1** also in MeCN/H_2O as shown in Fig. S18. A reversible redox wave was observed at –1.25 V (*vs.* Fc/Fc^+) and assigned as a 2e⁻ redox process, since the peak current in the DPV was almost doubled relative to that at +0.94 V. This result suggests that, after the proton-coupled 1e⁻ reduction of **1** to form $[Ru^{II}(tpphz\text{-}H^{•})(bpy)_2]^{2+}$, the subsequent 1e⁻-reduction of $[Ru^{II}(tpphz\text{-}H^{•})(bpy)_2]^{2+}$ occurs very fast to form **2** as shown in Scheme 3. We also scrutinized the reaction of $[Ru^{II}(tpphz\text{-}H^{•})(bpy)_2]^{2+}$ to form **2** by using nanosecond laser-flash photolysis of a CH_3OH-H_2O solution of **1** (25 μM) in the presence of excess Et_3N (100 mM) under photoexcitation at 426 nm. Formation of $[Ru^{II}(tpphz\text{-}H^{•})(bpy)_2]^{2+}$ was not observed in the presence of Et_3N, because the subsequent reaction to form **2** proceeds rapidly in the solvent cage without releasing detectable 1e⁻-reduced intermediates.

Subsequently, a H_2 molecule is formed *via* the reaction of the photoexcited intermediate of **2**, which is assumed to be the triplet MLCT excited state of **2** (^{3}**2***), with a proton present in the solvent. This assumption is supported by the requirement of photo-excitation of **2** for the hydrogen evolution (See the first paragraph of this section) and the dependence of the efficiency on proton concentration (Fig. S17). In addition, the slower rate and the KIE observed for the rate of the hydrogen evolution catalysed by **1** indicate that the RDS throughout all the process is the H-H bond formation between the intermediate **2** and a proton.

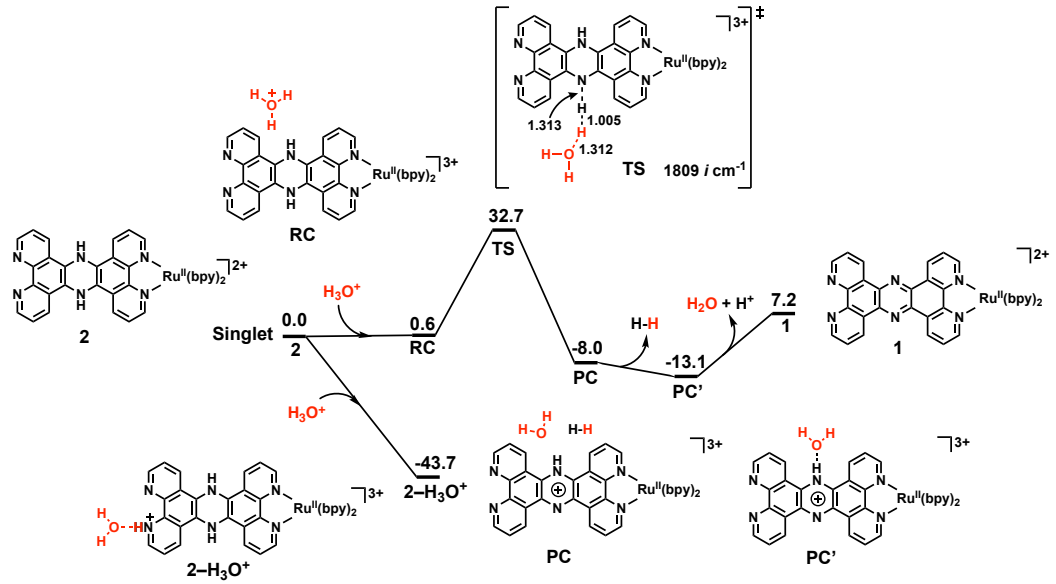

Fig. 11 Energy diagram (in units of kcal/mol) for the catalytic process from **2** to **1** in the singlet ground state computed at the B3LYP level of theory in water. **RC**: reactant complex, **TS**: transition state, and **PC**: product complex.

TD-DFT assessment on the photocatalytic H_2 evolution by 1.

The proposed mechanism of hydrogen evolution in the second half of the catalytic cycle is shown in Scheme 3. Fig. 11 shows a computed energy diagram for the reaction pathway from 2 to 1 in the hydrogen evolution process in the singlet ground state. The method of choice here is the B3LYP level of theory,[44-46] as mentioned in the figure caption. Solvent effects of water were considered by using the polarizable continuum model (PCM)[56] in the DFT calculations. When hydronium coordinates to a pyridine N atom, the reaction system of **2**-H_3O^+ is significantly stabilized in energy. As a result, this branch would not participate in the main reaction of hydrogen evolution. On the other hand, the attack of hydronium to a bridging NH of **2** in the initial stages of the reaction gives rise to hydrogen evolution with a water molecule *via* transition state (TS), which can connect reactant complex (RC) and product complex (PC). Hydronium or $H_2O + H^+$ is regenerated in the final stages of the reaction. However, the barrier height from RC to TS is computed to be 32.1 kcal/mol, which is considered to be too high for a thermal process. Clearly, this barrier is not thermally accessible at room temperature. Photoirradiation is therefore necessary for the reaction from **2** to **1** to take place through excited states.

We next carried out time-dependent density functional theory (TD-DFT)[57] calculations to have a better insight into the reaction mechanism of the photocatalytic H_2 evolution with **1** under visible-light irradiation. Fig. 12 shows a schematic representation of the photocatalytic process as a function of the reaction coordinate obtained from intrinsic reaction coordinate (IRC)[58] analysis with respect to **TS**. The ^{1}**R** species on the S_0 surface is initially photoexcited to the ^{1}**R*** species (on the S_2 surface), which lies 68.9 kcal/mol (2.93 eV) compared to the ^{1}**R** species. This process can occur in the vicinity of the reactant complex **RC** shown in Fig. 11 by the irradiation of visible light. The computational result in particular on the energy difference between ^{1}**R** and ^{1}**R*** is fully consistent with experiment.

Then, the ^{1}**R*** species on the S_2 surface is converted to the ^{3}**I*** species on the T_1 surface near the transition state **TS** shown in Fig. 11 *via* the first intersystem crossing (ISC). The ^{3}**I*** species moves to the ^{3}**P*** species on the T_1 surface. Finally, the ^{3}**P*** species comes down to the ^{1}**P** species on the S_0 surface *via* the second ISC. This process can occur in the vicinity of the product complex **PC** shown in Fig. 11. In this way visible-light irradiation, which is necessary for the photoexcitation of **RC**, is able to drive the reaction from **2** to **1** with hydrogen evolution.

Fig. 13 shows a computed UV-Vis absorption spectrum for reactant complex ^{1}**R**. The electron-density-difference pictures show that charge transfer occurs from the yellow regions to the light-blue regions. There are main two peaks at 430 and

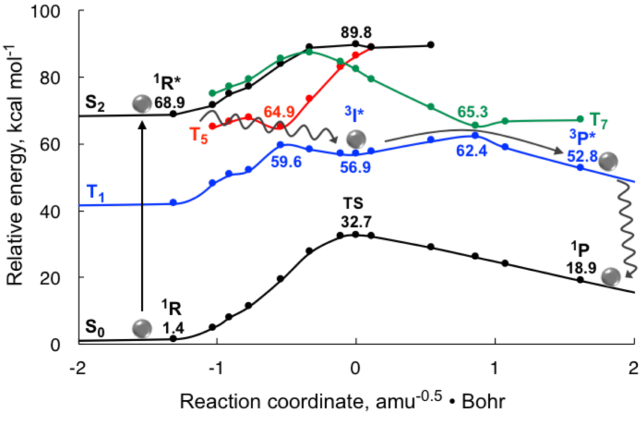

Fig. 12 Schematic representation of the photocatalytic process as a function of the reaction coordinate from **2** to **1**.

350 nm in the calculated spectrum. We see that metal-to-ligand charge transfer (MLCT) processes such as $1e^-$ excitations from HOMO–3 to LUMO+2 (f = 0.112), from HOMO–2 to LUMO+2 (f

= 0.096) and from HOMO–1 to LUMO+3 (f = 0.094) should significantly contribute to the main 430 nm peak. The first and second ones can be assigned to MLCT (bpy) and the third one MLCT (tpphz) on the basis of the electron-density-difference pictures. On the other hand, a 1e⁻ excitation from HOMO to LUMO+10 has large oscillator strength (f = 0.136) and it contributes to the 350 nm peak. This ET occurs within the tpphz ligand; it is assignable to the π-π* transition in Fig. 1. The small two peaks at 581 and 619 nm correspond to 1e⁻ excitations from HOMO to LUMO+3 and from HOMO to LUMO, respectively. The computed UV-Vis spectral shape is very similar to the observed one in this study.

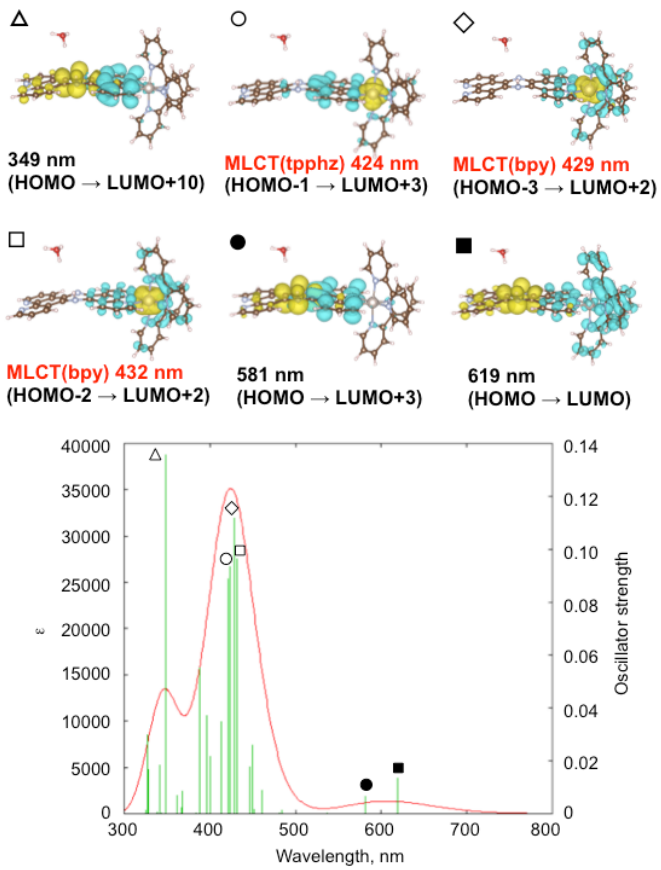

Fig. 13 Computed UV-Vis spectrum for **¹R** with electron-density-difference pictures. Light blue: electron-density increase, yellow: electron-density decrease. As a result of ET, the electron density of the light-blue regions is increased while that of the yellow regions is decreased. Absorptions shown in the calculated spectrum as triangle, circle, rectangle, square, filled circle, and filled square were assigned to respective transitions depicted as orbital distributions above.

Photocatalytic hydrogenation of organic substrates.

To explore further reactivity of the hydrogenated species **2**, photocatalytic hydrogenation of organic substrates was also examined with **1** as a catalyst in the presence of Et_3N as a sacrificial reductant. A CD_3OD solution of **1** (0.26 mM), benzaldehyde (0.14 M) and Et_3N (0.21 M) was irradiated with white light (380 – 670 nm) and the reaction was monitored with ^1H NMR spectroscopy. As a result, hydrogenation of benzaldehyde proceeded to give benzyl alcohol[59] as a product and the TON was determined to be 29 at 48 h (Fig. S20). The linearity of the time-course of the benzyl alcohol production clearly demonstrates the robustness of **1** as a photocatalyst for the hydrogenation. In sharp contrast, when an excess amount of benzaldehyde was added to the solution of **2**, which was formed under photoirradiation to the solution of **1**, and the mixture was kept in the dark, the ^1H NMR signals of **2** and benzaldehyde were intact even after 24 h. Therefore, the hydrogenation of organic substrates also requires further photoexcitation of **2**, as in the case of the photocatalytic hydrogen evolution mentioned above. Photocatalytic reduction of other organic substrates with **1** were also performed and only benzophenone, benzaldehyde and the derivatives were hydrogenated to give the corresponding benzhydrol and benzyl alcohol derivatives (Table S2).

Conclusions

Photocatalytic hydrogen evolution has been demonstrated in an aqueous media with use of **1**, having the π-expanded tpphz ligand, as a catalyst in the presence of an electron donor under white-light irradiation at room temperature. Photoirradiation of **1** in the presence of an electron donor allows us to observe the efficient and selective formation of the 2H-reduced complex **2**, whose pyrazine moiety in the tpphz ligand is dihydrogenated at the two nitrogen atoms, as clarified by ^1H and ^{15}N NMR spectroscopies. Complex **2** is selectively formed, through the formation of the short-lived 1e⁻-reduced species of **1**, as the sole product of photoinduced PCET, in which an electron is delivered from an electron donor and a proton from a protic solvent such as water as well as 1e⁻-oxidized species of the electron donor to show an inverse KIE. The important point of the characteristics of **2** is that the N-H proton can bear a hydride character in the photoexcited state to react with proton to afford H_2 and to hydrogenate carbonyl groups. It should be noted that the detection of an intermediate in photocatalytic hydrogen evolution has been seldom reported and the clear elucidation on the formation mechanism of such an intermediate would be valuable for the development of efficient photocatalytic hydrogen-evolving system. The plausible mechanism of hydrogen evolution has been revealed to involve a photoinduced reaction of **2** with a proton to form the H-H bond, *i.e.* H_2, as the final rate-limiting step in the hydrogen evolution, to show a normal KIE. As for catalytic hydrogen evolution reactions, it is very rare that the catalytic centre is not the metal centre to generate metal-hydride intermediates[60] but an organic ligand.[30] The results presented herein would be suggestive for mechanistic insight into photocatalytic hydrogen evolution using heteroaromatic materials including semiconducting melem polymers[61] and triphenylarenes.[62] The fact that a heteroaromatic ligand can act as an active site for the hydrogen evolution reaction suggests that facile adjustment of the properties of organic ligands should be effective to develop more efficient catalytic systems based on Ru^{II}-polypyridine complexes. In addition, the intermediates of photocatalytic hydrogen evolution can be applied to efficient photocatalytic hydrogenation of organic substrates, as demonstrated in this study.

Experimental

General.

All reactions and measurements were carried out under argon. $[Ru^{II}(bpy)_2(tpphz)](ClO_4)_2$ (**1**·$(ClO_4)_2$),[31] $[Ru^{II}(bpy)_2$-$(taptp)](ClO_4)_2$ (taptp = 4,5,9,18-tetraaza-phenanthreno[9,10-*b*]triphenylene, **3**·$(ClO_4)_2$),[54] $[Ru^{II}(bpy)_3](ClO_4)_2$ (**4**·$(ClO_4)_2$)[63] and $[Ru^{II}(bpy)_2(bpm)](ClO_4)_2$ (**5**·$(ClO_4)_2$)[64] were synthesized according to the literature methods. NMR measurements were performed on a Bruker AVANCE-600 spectrometer. Chemical shifts of ^{15}N NMR spectra were calibrated relative to that of an external reference of $(^{15}NH_4)_2SO_4$ (δ 20.55 ppm)[41] in H_2O. UV-vis absorption spectra were recorded with use of Shimadzu UV-3600 and UV-2450 spectrometers. Emission spectra were recorded on a HORIBA FluoroMax-4 spectrometer. Electrochemical measurements were performed using a BAS ALS-710D electrochemical analyser. A decay curve of phosphorescence intensity of **1**·$(ClO_4)_2$ was obtained using a HORIBA Fluorolog-3 + DeltaFlex/Pro spectrometer. Gas chromatography was performed on a Shimadzu GC-2014 equipped with a thermal conductivity detector (TCD) and a capillary column packed with molecular sieves 5A. ESI-TOF- and GC-MS(EI) spectra were measured on JEOL JMS-T100CS and SHIMADZU GC-2010 Plus spectrometers, respectively. Photoirradiation of the sample was performed by using a Xe light source (300 W) on an ASAHI SPECTRA MAX-301 at room temperature. Dynamic light scattering (DLS) was measured on an Otsuka electronics FDLS-3000.

Synthesis.

Formation of 2·$(ClO_4)_2$. The reaction to form **2** and its NMR measurements were performed in a sealed NMR tube under Ar. A white light (380 – 670 nm) was irradiated to the solution containing **1**·$(ClO_4)_2$ (0.3 mM) and Et_3N (71 mM) in CD_3OD : D_2O mixed solvent (1:1, v/v, 0.7 mL) for 30 min under Ar at room temperature. After photoirradiation, the ^1H NMR spectrum of the sample was directly measured at room temperature without isolation of **2**. ^1H NMR (CD_3OD : D_2O = 1 : 1, v/v): δ8.98 (d, *J* = 5.0 Hz, 2H; tpphz-Ha), 8.75 (d, *J* = 8.2 Hz, 4H; tpphz-Ha' and bpy-H3), 8.72 (d, *J* = 8.0 Hz, 2H; bpy-H3'), 8.62 (dd, *J* = 5.0, 1.2 Hz, 2H; tpphz-Hc'), 8.18 (td, *J* = 8.0, 1.4 Hz, 2H; bpy-H4), 8.10 (td, *J* = 8.0, 1.2 Hz, 2H; bpy-H4'), 8.01 (t, *J* = 5.3 Hz, 2H; tpphz-Hc), 7.96 (dd, *J* = 5.5, 1.0 Hz, 2H; bpy-H6'), 7.83 - 7.77 (m, 4H; tpphz-Hb and tpphz-Hb'), 7.70 (dd, *J* = 8.0, 1.5 Hz, 2H; bpy-H6), 7.55 (td, *J* = 7.9, 1.4 Hz, 2H; bpy-H5), 7.39 (td, *J* = 8.0, 1.4 Hz, 2H; bpy-H5').

Formation of (2-^{15}N)·Cl_2. The synthetic procedure of ^{15}N-labelled **1**·$(ClO_4)_2$ ((**1**-^{15}N)·$(ClO_4)_2$) and the ion-exchange method to obtain (**1**-^{15}N)·Cl_2 are described in the ESI. The reaction to form (**2**-^{15}N)·Cl_2 was performed in a sealed NMR tube under Ar at room temperature. The solution containing (**1**-^{15}N)·Cl_2 (1 mM) and Et_3N (0.2 M) in a CH_3OH-benzene-d_6 mixed solvent (0.7 mL, 9:1, v/v) was irradiated by white light (380 – 670 nm) for 4 h under Ar. After photoirradiation, the ^{15}N NMR spectrum of the sample was directly measured at room temperature without isolation of (**2**-^{15}N)·Cl_2. ^{15}N NMR (CH_3OH : benzene-d_6 = 9 : 1 v/v, at 195 K): δ73.43 (d, J_{NH} = 81.6 Hz).

Measurements.

Photocatalytic hydrogen evolution catalysed by 1·$(ClO_4)_2$. Photocatalytic hydrogen evolution was carried out at room temperature in a quartz cuvette with five transparent faces (cell volume: 5.34 mL), which was capped by a rubber septum and whose inside was filled with Ar. Before photoirradiation, the solution (total volume: 4 mL) was degassed by bubbling with Ar for 30 min. A white light in the range of 380 – 670 nm, which was generated from a Xe lamp equipped with a mirror module to remove the UV light, was irradiated to the cuvette from the underneath with a path length of 4 cm. After photoirradiation, 0.1 mL of the gas phase in the cell was taken with a gas-tight syringe and analysed by GC.

Photoelectrocatalytic hydrogen evolution catalysed by 1·$(ClO_4)_2$. Photoelectrocatalytic hydrogen evolution was carried out at room temperature in a sealed reaction vessel, equipped with three electrodes and separated to two cells by a membrane (Fig. S21). The light source used for the photocatalytic hydrogen evolution was also employed here (See above). Degassing and monitoring the reaction products were performed with the same procedure for the photocatalytic hydrogen evolution (See above).

ns-Laser flash photolysis measurements. Nanosecond time-resolved transient absorption measurements were performed using a laser system provided by UNISOKU Co., Ltd. according to the following procedure. A deaerated mixture solution in a quartz cell (1 cm × 1 cm) was excited by a Nd:YAG laser (Continuum SLII-10, 4-6 ns fwhm, λ_{ex} = 426 nm, 10 mJ pulse^{-1}). The photodynamics was monitored by continuous exposure to a xenon lamp for the visible region and halogen lamp for the near-IR region as a probe light and a photomultiplier tube (Hamamatsu 2949) as a detector.

Hydrogenation of organic substrates by 1·$(ClO_4)_2$. Photocatalytic hydrogenation of organic substrates was performed at room temperature under Ar in NMR tubes, which were capped by a rubber septum. The solution containing **1**·$(ClO_4)_2$ (0.26 mM), a substrate (0.14 M), Et_3N (0.21 M) and sodium 4,4-dimethyl-4-silapentane-1-sulfonate (DSS) (0.10 mM) in CD_3OD was transferred to an NMR tube and degassed by bubbling with Ar for 30 min. A white light (380 – 670 nm) was irradiated to the NMR tube. The amounts of the substrate and the corresponding products after photoirradiation were determined on the basis of the integral values of the signals in the ^1H NMR spectra after photoirradiation, with use of DSS as an internal standard.

DFT calculations.

Density functional theory (DFT) and time-dependent density functional theory (TD-DFT)[57] calculations were performed by using the Gaussian 09 program.[65] The method of choice is the B3LYP level of theory[44-46] combined with the SDD basis set[47] for the Ru atom and the D95** basis set[48] for the other atoms. Solvent effects of water (dielectric constant = 78.36) were considered by using the polarizable continuum model (PCM)[56] in the DFT calculations. Cartesian coordinates of all the geometry-optimized reaction species are given in Table S3.

First, we optimized the transition-state structure (**TS**) and then obtained the minimum energy pathway (MEP) connecting **2** and **1** *via* **TS** using intrinsic reaction coordinate (IRC)[58] analysis. After that, we performed TD-DFT calculations at sampling

points along the MEP to have excited states of spin singlet (S_N) about N = 1-30. Next, we calculated single-point calculations of spin triplet using the sampling points along the MEP to obtain the T_1 pathway. Then we obtained the T_N pathways about N = 2-31 using TD-DFT calculations. Graphics of all the obtained structures were produced by using VESTA.[66] To analyse the electronic distribution of the excited states, the electron density difference maps were visualized by using the GaussSum 3.0 program.[67]

Conflicts of interest

There are no conflicts to declare.

Acknowledgements

This work was partially supported by Grants-in-Aid (Nos. 24245011, 15H00861 and 15H00915 (AnApple) to T. K., and No. 16H02268 to S.F.) and 24-2397 (T. S.) from the Japan Society of Promotion of Science of Japan. T. K. also appreciates financial support from The Mitsubishi Foundation and Yazaki Memorial Foundation for Science and Technology. K. Y. thanks MEXT projects Integrated Research Consortium on Chemical Sciences, Cooperative Research Program of Network Joint Research Centre for Materials and Devices, Elements Strategy Initiative to Form Core Research Centre, JST-CREST JPMJCR15P5 and JST-Mirai JPMJMI18A2 for their financial support. The computations were mainly carried out by using the computer facilities at Research Institute for Information Technology, Kyushu University.

Notes and references

1 (a) E. Borgarello, J. Kiwi, E. Pelizzetti, M. Visca and M. Grätzel, *J. Am. Chem. Soc.,* 1981, **103**, 6324-6329; (b) J. I. Goldsmith, W. R. Hudson, M. S. Lowry, T. H. Anderson and S. Bernhard, *J. Am. Chem. Soc.,* 2005, **127**, 7502-7510.
2 (a) T. Lazarides, T. McCormick, P. Du, G. Luo, B. Lindley and R. Eisenberg, *J. Am. Chem. Soc.,* 2009, **131**, 9192-9194; (b) L. Tong, R. Zong and R. P. Thummel, *J. Am. Chem. Soc.,* 2014, **136**, 4881-4884.
3 S. J. Hwang, D. C. Powers, A. G. Maher and D. G. Nocera, *Chem. Sci.,* 2015, **6**, 917-922.
4 (a) D. Ravelli, D. Dondi, M. Fagnoni and A. Albini, *Chem. Soc. Rev.,* 2009, **38**, 1999-2011; (b) F. Mahdavi, T. C. Bruton and Y. Li, *J. Org. Chem.,* 1993, **58**, 744-746.
5 V. Balzani, A. Credi and M. Venturi, *ChemSusChem,* 2008, **1**, 26-58.
6 S. Fukuzumi, *Bull. Chem. Soc. Jpn.,* 1997, **70**, 1-28.
7 (a) J. K. Matsui, S. B. Lang, D. R. Heitz and G. A. Molander, *ACS Catal.,* 2017, **7**, 2563-2575; (b) T. Koike and M. Akita, *Inorg. Chem. Front.,* 2014, **1**, 562-576; (c) K. Zeitler, *Angew. Chem., Int. Ed.,* 2009, **48**, 9785-9789; (d) D. A. Nicewicz and D. W. C. MacMillan, *Science,* 2008, **322**, 77-80.
8 (a) N. Serpone, E. Pelizzetti and M. Grätzel, *Coord. Chem. Rev.,* 1985, **64**, 225-245; (b) N. D. McClenaghan, Y. Leydet, B. Maubert, M. T. Indelli and S. Campagna, *Coord. Chem. Rev.,* 2005, **249**, 1336-1350; (c) B. Happ, A. Winter, M. D. Hager and U. S. Schubert, *Chem. Soc. Rev.,* 2012, **41**, 2222-2255.
9 (a) O. S. Wenger, *Acc. Chem. Res.,* 2013, **46**, 1517-1526; (b) M. H. V. Huynh, D. M. Dattelbaum and T. J. Meyer, *Coord. Chem. Rev.,* 2005, **249**, 457-483; (c) B. Elias and A. Kirsch-De Mesmaeker, *Coord. Chem. Rev.,* 2006, **250**, 1627-1641.
10 (a) C. A. Bignozzi, R. Argazzi, C. Chiorboli, S. Roffia and F. Scandola, *Coord. Chem. Rev.,* 1991, **111**, 261-266; (b) L. Hammarström, *Acc. Chem. Res.,* 2015, **48**, 840-850; (c) M. D. Kärkäs, E. V. Johnston, O. Verho and B. Åkermark, *Acc. Chem. Res.,* 2014, **47**, 100-111.
11 A. Juris, V. Balzani, F. Barigelletti, S. Campagna, P. Belser and A. von Zelewsky, *Coord. Chem. Rev.,* 1988, **84**, 85-277.
12 (a) D. W. Thompson, A. Ito and T. J. Meyer, *Pure Appl. Chem.,* 2013, **85**, 1257-1305; (b) N. Sutin and C. Creutz, *Pure Appl. Chem.,* 1980, **52**, 2717-2738; (c) T. J. Meyer, *Acc. Chem. Res.,* 1989, **22**, 163-170.
13 J. L. Dempsey, J. R. Winkler and H. B. Gray, *Chem. Rev.,* 2010, **110**, 7024-7039.
14 (a) B. Durham, J. V. Caspar, J. K. Nagle and T. J. Meyer, *J. Am. Chem. Soc.,* 1982, **104**, 4803-4810; (b) N. H. Damrauer, G. Cerullo, A. Yeh, T. R. Boussie, C. V. Shank and J. K. McCusker, *Science,* 1997, **275**, 54-57; (c) A. W. Adamson and J. N. Demas, *J. Am. Chem. Soc.,* 1971, **93**, 1800-1801.
15 (a) C. R. Bock, T. J. Meyer and D. G. Whitten, *J. Am. Chem. Soc.,* 1974, **96**, 4710-4712. (b) C. Creutz, N. Sutin and B. S. Brunschwig, *J. Am. Chem. Soc.,* 1979, **101**, 1297-1298.
16 (a) D. W. Low, J. R. Winkler and H. B. Gray, *J. Am. Chem. Soc.,* 1996, **118**, 117-120; (b) J. Berglund, T. Pascher, J. R. Winkler and H. B. Gray, *J. Am. Chem. Soc.,* 1997, **119**, 2464-2469.
17 (a) S. Fukuzumi, T. Kishi, H. Kotani, Y.-M. Lee and W. Nam, *Nat. Chem.,* 2011, **3**, 38-41; (b) H. Kotani, T. Suenobu, Y.-M. Lee, W. Nam and S. Fukuzumi, *J. Am. Chem. Soc.,* 2011, **133**, 3249-3251; (c) S. Ohzu, T. Ishizuka, Y. Hirai, S. Fukuzumi and T. Kojima, *Chem.–Eur. J.,* 2013, **19**, 1563-1567.
18 (a) M. Yagi and M. Kaneko, *Chem. Rev.,* 2001, **101**, 21-36; (b) C. Panda, J. Debgupta, D. Díaz Díaz, K. K. Singh, S. Sen Gupta and B. B. Dhar, *J. Am. Chem. Soc.,* 2014, **136**, 12273-12282; (c) T. Ishizuka, A. Watanabe, H. Kotani, D. Hong, K. Satonaka, T. Wada, Y. Shiota, K. Yoshizawa, K. Ohara, K. Yamaguchi, S. Kato, S. Fukuzumi and T. Kojima, *Inorg. Chem.,* 2016, **55**, 1154-1164.
19 (a) J. Kiwi and M. Grätzel, *Nature,* 1979, **281**, 657-658; (b) P. J. DeLaive, B. P. Sullivan, T. J. Meyer and D. G. Whitten, *J. Am. Chem. Soc.,* 1979, **101**, 4007-4008; (c) M. A. Gross, A. Reynal, J. R. Durrant and E. Reisner, *J. Am. Chem. Soc.,* 2014, **136**, 356-366.
20 (a) G. M. Brown, B. S. Brunschwig, C. Creutz, J. F. Endicott and N. Sutin, *J. Am. Chem. Soc.,* 1979, **101**, 1298-1300; (b) G. M. Brown, S. F. Chan, C. Creutz, H. A. Schwarz and N. Sutin, *J. Am. Chem. Soc.,* 1979, **101**, 7638-7640; (c) S. F. Chan, M. Chou, C. Creutz, T. Matsubara and N. Sutin, *J. Am. Chem. Soc.,* 1981, **103**, 369-379; (d) C. V. Krishnan and N. Sutin, *J. Am. Chem. Soc.,* 1981, **103**, 2141-2142.
21 (a) C. Pac, M. Ihama, M. Yasuda, Y. Miyauchi and H. Sakurai, *J. Am. Chem. Soc.,* 1981, **103**, 6495-6497; (b) S. Fukuzumi, S. Koumitsu, K. Hironaka and T. Tanaka, *J. Am. Chem. Soc.,* 1987, **109**, 305-316; (c) S. Fukuzumi, S. Mochizuki and T. Tanaka, *J. Phys. Chem.,* 1990, **94**, 722-726.
22 (a) T. Fukushima, T. Wada, H. Ohtsu and K. Tanaka, *Dalton Trans.,* 2010, **39**, 11526-11534; (b) S. K. Padhi and K. Tanaka, *Inorg. Chem.,* 2011, **50**, 10718-10723; (c) K. Kobayashi, H. Ohtsu, K. Nozaki, S. Kitagawa and K. Tanaka, *Inorg. Chem.,* 2016, **55**, 2076-2084.
23 (a) M. H. V. Huynh and T. J. Meyer, *Chem. Rev.,* 2007, **107**, 5004-5064; (b) C. J. Gagliardi, B. C. Westlake, C. A. Kent, J. J. Paul, J. M. Papanikolas and T. J. Meyer, *Coord. Chem. Rev.,* 2010, **254**, 2459-2471; (c) D. R. Weinberg, C. J. Gagliardi, J. F. Hull, C. F. Murphy, C. A. Kent, B. C. Westlake, A. Paul, D. H. Ess, D. G. McCafferty and T. J. Meyer, *Chem. Rev.,* 2012, **112**, 4016-4093.

24 (a) J. J. Warren, T. A. Tronic and J. M. Mayer, *Chem. Rev.,* 2010, **110**, 6961-7001; (b) J. M. Mayer, *Acc. Chem. Res.,* 2011, **44**, 36-46.
25 (a) S. Hammes-Schiffer, *Acc. Chem. Res.,* 2009, **42**, 1881-1889; (b) S. Hammes-Schiffer, E. Hatcher, H. Ishikita, J. H. Skone and A. V. Soudackov, *Coord. Chem. Rev.,* 2008, **252**, 384-394.
26 (a) J. J. Concepcion, M. K. Brennaman, J. R. Deyton, N. V. Lebedeva, M. D. E. Forbes, J. M. Papanikolas and T. J. Meyer, *J. Am. Chem. Soc.,* 2007, **129**, 6968-6969; (b) N. V. Lebedeva, R. D. Schmidt, J. J. Concepcion, M. K. Brennaman, I. N. Stanton, M. J. Therien, T. J. Meyer and M. D. E. Forbes, *J. Phys. Chem. A,* 2011, **115**, 3346-3356.
27 (a) D. E. Polyansky, D. Cabelli, J. T. Muckerman, E. Fujita, T. Koizumi, T. Fukushima, T. Wada and K. Tanaka, *Angew. Chem., Int. Ed.,* 2007, **46**, 4169-4172; (b) D. E. Polyansky, D. Cabelli, J. T. Muckerman, T. Fukushima, K. Tanaka and E. Fujita, *Inorg. Chem.,* 2008, **47**, 3958-3968; (c) T. Fukushima, E. Fujita, J. T. Muckerman, D. E. Polyansky, T. Wada and K. Tanaka, *Inorg. Chem.,* 2009, **48**, 11510-11512; (d) H. Ohtsu and K. Tanaka, *Angew. Chem., Int. Ed.,* 2012, **51**, 9792-9795.
28 (a) K. Yamada, K. Katsuura, H. Kasimura and H. Iida, *Bull. Chem. Soc. Jpn.,* 1976, **49**, 2805-2810; (b) R. Wang, T. Okajima, F. Kitamura, S. Kawauchi, N. Matsumoto, T. Thiemann, S. Mataka and T. Ohsaka, *J. Phys. Chem. A,* 2004, **108**, 1891-1899.
29 T. G. Dunne and J. K. Hurst, *Inorg. Chem.,* 1980, **19**, 1152-1157.
30 (a) T. Matsumoto, H.-C. Chang, M. Wakizaka, S. Ueno, A. Kobayashi, A. Nakayama, T. Taketsugu and M. Kato, *J. Am. Chem. Soc.,* 2013, **135**, 8646-8654; (b) K. Koshiba, K. Yamauchi and K. Sakai, *Angew. Chem., Int. Ed.,* 2017, **56**, 4247-4251.
31 J. Bolger, A. Gourdon, E. Ishow and J.-P. Launay, *Inorg. Chem.,* 1996, **35**, 2937-2944.
32 (a) J. Bolger, A. Gourdon, E. Ishow and J.-P. Launay, *J. Chem. Soc., Chem. Commun.,* 1995, 1799-1800; (b) Y. Sun, D. A. Lutterman and C. Turro, *Inorg. Chem.,* 2008, **47**, 6427-6434.
33 The small wave observed at –0.8 V *vs.* SCE in the CV (Fig. S1) was derived from O_2 reduction from air.
34 C. Chiorboli, C. A. Bignozzi, F. Scandola, E. Ishow, A. Gourdon and J.-P. Launay, *Inorg. Chem.,* 1999, **38**, 2402-2410.
35 B. Valeur, *Molecular Fluorescence: Principles and Applications*; Wiley-VCH, Weinheim, 2002.
36 (a) M. Kirch, J.-M. Lehn and J.-P. Sauvage, *Helv. Chim. Acta,* 1979, **62**, 1345-1384; (b) M. Dossot, X. Allonas and P. Jacques, *J. Photochem. Photobiol. A*, 1999, **128**, 47-55; (c) O. Poizat, G. Buntinx and L. Boilet, *J. Phys. Chem. A*, 2005, **109**, 10813-10823.
37 G. Gauglitz, in *Photochromism Molecules and Systems, Revised Edition*; H. Dürr, H. Bouas-Laurent eds.; Elsevier; Amsterdam, 2003; p. 30.
38 S. K. Padhi, R. Fukuda, M. Ehara and K. Tanaka, *Inorg. Chem.,* 2012, **51**, 8091-8102.
39 Complex **2**, formed in the presence of Ox as the electron donor, seems non-emissive (Fig. S6).
40 The formation reaction of **2** by photoirradiation to the solution of **1** including Et_3N as an electron donor was too fast to monitor the time course by UV-Vis spectroscopy; however, the reactions with Ox, EtMor or triethanolamine (TEOA) were slow enough to monitor and the spectral changes exhibited isosbestic points at 473 nm for Ox, 510 nm for EtMor, and 509 nm for TEOA (Fig. S7).
41 M. Alei, L. O. Morgan, W. E. Wageman and T. W. Whaley, *J. Am. Chem. Soc.,* 1980, **102**, 2881-2887.
42 (a) S. Kakuda, R. L. Peterson, K. Ohkubo, K. D. Karlin and S. Fukuzumi, *J. Am. Chem. Soc.,* 2013, **135**, 6513-6522; (b) T. Tano, Y. Okubo, A. Kunishita, M. Kubo, H. Sugimoto, N. Fujieda, T. Ogura and S. Itoh, *Inorg. Chem.,* 2013, **52**, 10431-10437.
43 M. Inamo, S. Funahashi and M. Tanaka, *Bull. Chem. Soc. Jpn.,* 1986, **59**, 2629-2630.
44 A. D. Becke, *Phys. Rev. A,* 1988, **38**, 3098–3100.
45 C. Lee, W. Yang and R. G. Parr, *Phys. Rev. B,* 1988, **37**, 785–789.
46 A. D. Becke, *J. Chem. Phys.,* 1993, **98**, 5648-5652.
47 D. Andrae, U. Häußermann, M. Dolg, H. Stoll and H. Preuß, *Theor. Chem. Acc.,* 1990, **77**, 123-141.
48 T. H. Dunning and P. J. Hay, In *Modern Theoretical Chemistry*; H. F. Schaefer, III, Ed.; Plenum: New York, 1976; Vol. 3, pp 1–27.
49 (a) J. M. Camara and T. B. Rauchfuss, *J. Am. Chem. Soc.,* 2011, **133**, 8098-8101; (b) H. Kotani, R. Hanazaki, K. Ohkubo, Y. Yamada and S. Fukuzumi, *Chem.–Eur. J.,* 2011, **17**, 2777-2785.
50 J. Park, Y. Morimoto, Y.-M. Lee, W. Nam and S. Fukuzumi, *Inorg. Chem*., 2014, **53**, 3618-3628.
51 Ru^{II}-tpphz complexes, having a Pd^{II} or Pt^{II} complex moiety as a catalytic active site for photochemical hydrogen evolution, have been also reported. (a) S. Rau, B. Schäfer, D. Gleich, E. Anders, M. Rudolph, M. Friedrich, H. Görls, W. Henry and J. G. Vos, *Angew. Chem., Int. Ed.,* 2006, **45**, 6215-6218; (b) S. Tschierlei, M. Karnahl, M. Presselt, B. Dietzek, J. Guthmuller, L. González, M. Schmitt, S. Rau and J. Popp, *Angew. Chem., Int. Ed.,* 2010, **49**, 3981-3984; (c) M. G. Pfeffer, T. Kowacs, M. Wächtler, J. Guthmuller, B. Dietzek, J. G. Vos and S. Rau, *Angew. Chem., Int. Ed.,* 2015, **54**, 6627-6631.
52 B. S. Winkler, S. M. Orselli and T. S. Rex, *Free Radical Biol. Med.* 1994, **17**, 333-349.
53 (a) C. G. Morales-Guio, L. Liardet, M. T. Mayer, S. D. Tilley, M. Grätzel and X. Hu, *Angew. Chem., Int. Ed.,* 2015, **54**, 664-667; (b) C. L. Pitman and A. J. M. Miller, *ACS Catal.,* 2014, **4**, 2727-2733.
54 Y. Liu, A. Chouai, N. N. Degtyareva, D. A. Lutterman, K. R. Dunbar and C. Turro, *J. Am. Chem. Soc.,* 2005, **127**, 10796-10797.
55 Hydrogen evolution from π-conjugated organic compounds, which involves aromatization or extension of π-conjugation, frequently requires photoexcitation. See ref. 30 and K. Ujike, S. Kudoh and M. Nakata, *Chem. Phys. Lett.,* 2004, **396**, 288-292.
56 J. Tomasi, B. Mennucci and R. Cammi, *Chem. Rev.,* 2005, **105**, 2999–3094.
57 M. E. Casida, C. Jamorski, K. C. Casida and D. R. Salahub, *J. Chem. Phys.,* 1998, **108**, 4439-4449.
58 K. Fukui, *J. Phys. Chem.,* 1970, **74**, 4161-4163.
59 Since CD_3OD was used as the solvent, the obtained benzyl alcohol was deuterated to be C_6H_5CHDOD and a singlet ^1H NMR signal of the benzyl proton was observed at 4.64 ppm. Additionally, the GC-MS(EI) analysis of the reaction mixture after the photoirradiation afforded two peaks at 5.32 and 6.19 min of the retention time, which matches to the GC of an authentic benzyl alcohol (Fig. S19).
60 (a) A. J. Esswein and D. G. Nocera, *Chem. Rev.,* 2007, **107**, 4022-4047; (b) S. Fukuzumi and T. Suenobu, *Dalton Trans.,* 2013, **42**, 18-28.
61 X. Wang, K. Maeda, A. Thomas, K. Takanabe, G. Xin, J. M. Carlsson, K. Domen and M. Antonietti, *Nat. Mater.,* 2009, **8**, 76-80.
62 V. S. Vyas, F. Haase, L. Stegbauer, G. Savasci, F. Podjaski, C. Ochsenfeld and B. V. Lotsch, *Nat. Commun.,* 2015, **6**, 8508.
63 J. A. Broomhead, C. G. Young and P. Hood, In *Inorg. Synth.*; John Wiley & Sons, Inc., 2007; pp 338-340.
64 O. Hamelin, M. Rimboud, J. Pécaut and M. Fontecave, *Inorg. Chem.,* 2007, **46**, 5354-5360.
65 M. J. Frisch, *et al.* Gaussian 09, revision E.01; Gaussian, Inc.: Wallingford, CT, 2010. Full author list is shown in ESI.
66 K. Momma and F. Izumi, *J. Appl. Crystallogr*. 2011, **44**, 1272-1276.
67 N. M. O'Boyle, A. L. Tenderholt and K. M. Langner, *J. Comput. Chem.*, 2008, **29**, 839-845.
68

